Experimental Measurement of Dynamic Effect in Capillary Pressure Relationship for Two-Phase Flow in Weakly Layered Porous Media

Diganta Bhusan Das
Dept. of Chemical Engineering, Loughborough University, Loughborough LE11 3TU, U.K.

Mahsanam Mirzaei
Dept. of Engineering Science, University of Oxford, Oxford, OX1 3PJ, U.K.

DOI 10.1002/aic.13925
Published online October 9, 2012 in Wiley Online Library (wileyonlinelibrary.com).

Well-defined laboratory experiments have been conducted to determine the significance of dynamic effect in capillary pressure relationships for two-phase flow in weakly heterogeneous (layered) porous media. The heterogeneous layers are composed of a fine sand layer sandwiched between two coarse sand layers. Dynamic and quasi-static capillary pressure–saturation (P^c–S) and $\partial S/\partial t$–t relationships are determined, which are then used to determine the dynamic effect, indicated by a dynamic coefficient (τ). As well known, τ establishes the speed at which flow equilibrium ($\partial S/\partial t = 0$) is reached. In consistent with previous studies, τ is found to be a nonlinear function of saturation that depends on the medium permeability and the intensity of heterogeneity. τ values increase in the regions of less permeability (fine sand) in the domain. However, the τ–S functional dependence follows similar trends at different locations within the domain including regions of different permeability. We argue that saturation weighted average of local τ–S curves can be used as an effective τ–S curve for the whole domain which, when done, follows an exponential trend too. The effective τ–S curves suggest that the effective τ values for the porous layers lie between the τ values of coarse and fine sands at the same water saturation, and it is dominated by the τ values of coarse sand as it occupied the maximum volume of the domain. *AIChE J,* 59: 1723–1734, 2013
Keywords: two-phase flow, porous medium, heterogeneity, layers, capillary pressure, saturation, dynamic effect, dynamic coefficient

Introduction

The fluid flow processes in porous media are determined by the interplay of various forces (e.g., pressure, gravitational, and viscous forces) and factors such as temperature, medium permeability, and heterogeneity.[1–8] In the case of single-phase flow in porous media, the flow behavior is generally described by the Darcy law[9,10]

$$\overline{q} = -\frac{K}{\mu}\nabla P \tag{1}$$

where pressure gradient ∇P is the driving force, $\overline{q}$ is the Darcy flux defined as the flow rate per unit cross-sectional area, μ is the fluid viscosity, and K is the intrinsic permeability of the porous medium. In the case of saturated two-phase flow in porous media, Eq. 1 can be extended based on various assumptions including that the driving force for the fluid phases is determined by the gradient in phase pressures for that particular phase and other forces such as gravity. The extended form of Darcy's law for two-phase flow can be expressed in the following form

$$\overline{q}_\gamma = -\frac{K_{r\gamma}K}{\mu}\left(\nabla \mathrm{P}_\gamma + \rho_\gamma g \nabla z\right), \quad \gamma \equiv \text{nonwetting fluid (nw) or wetting fluid (w)} \tag{2}$$

where ∇z is the upward unit vector, ρ_γ is the fluid density, and $K_{r\gamma}$ is the relative permeability. When the pore space is occupied by two immiscible fluid phases, an interface exists between the two phases. The pressures in the two phases near the interface will not be the same, and a pressure difference will exist across the interface. This pressure difference is referred to as capillary pressure (P^c). In the context of two-phase flow in porous medium, P^c is the pressure required to drive a fluid through the pores and displace the pore-wetting fluid. For example, as the pore size becomes smaller, higher capillary pressures are generally required to displace fluids. Therefore, in the description of two-phase flow in porous media, capillary forces play a central role. The main theoretical tool currently used to quantify the capillary pressure function is an empirical relationship obtained under equilibrium conditions between the average pressures of the individual phase in the form of[10]

Correspondence concerning this article should be addressed to D. B. Das at D.B.Das@lboro.ac.uk.

$$P_{nw} - P_w = P^{c,equ} = f(S) \quad (3)$$

where P_{nw} and P_w are the average pressures of the nonwetting and wetting phases, respectively, and S is the wetting phase saturation. As discussed by various authors (e.g., Das et al.[4]), Eq. 3 is defined to account for any parameter that influences the equilibrium distribution of the fluid phases in the porous domain. However, it has been shown that the fluid phases do not necessarily flow under steady condition ($\partial S/\partial t = 0$), particularly at smaller time periods when the time derivative of saturation ($\partial S/\partial t$) may not be ignored.[4,6,7] This fact has been supported by a number of experimental and modeling studies that show that the capillary pressure relationships depend on the flow conditions, that is, whether it is at steady or unsteady state.[7,11,12] Consequently, there are many authors who suggest that the conventional steady-state capillary pressure relationship (Eq. 3), which defines that P^c is a function of fluid equilibrium saturation alone, must be modified to account for the two-phase flow behavior under dynamic conditions.[5,7,13,14] To take into account, the dynamic capillary pressure effects on two-phase flow in porous media, Hassanizadeh and Gray[13] proposed a relationship, which indicates that the conventional P^c–S relationships (Eq. 3) can be generalized to include a capillary damping or dynamic coefficient τ as follows

$$\left(P^{c,dyn} - P^{c,equ}\right)\big|_s = -\tau(\partial S/\partial t)|_s \quad (4)$$

where $P^{c,dyn}$ is the dynamic capillary pressure ($P_{nw}^{dyn} - P_w^{dyn}$), $P^{c,equ}$ is the capillary pressure at equilibrium conditions ($P_{nw}^{equ} - P_w^{equ}$), which is calculated from Eq. (4), and $\partial S/\partial t$ is the time derivative of saturation, all measured at the same fluid saturation value (S). As evident, Eq. 4 has the general form of a straight line, and it should pass through the origin in this form. The slope of this linear relationship is the capillary damping coefficient or the dynamic coefficient (τ). If τ is small, the equivalence between $P^{c,dyn}$ and $P^{c,equ}$ is established quickly. On the other hand, the necessary time period to reach the equilibrium is high for larger τ values. Thus, the dynamic coefficient (τ) behaves as a capillary damping coefficient and indicates the dynamics of the two-phase flow system. In the last decade or so, there have been significant interests in determining the range of validity of Eq. 4 as well as obtaining τ values under different situations.[4–7,11–23] For example, τ has been shown to depend on the medium and fluid properties,[4,18,20] degree of heterogeneity,[4,21] wettability and contact angles in porous medium,[14] temperature,[6,22] and scales.[23] The dynamic capillary pressure relationship has been studied further using thermodynamically constrained averaging theory[24] where the effects of interfacial area between fluid phases have been discussed. The significance of the dynamic capillary pressure effect is also evidenced by the fact that a number of recent studies have focussed on developing numerical simulators[25–27] and artificial neural network tools[8] for two-phase flow in porous media based on the dynamic capillary pressure relationship (Eq. 4).

Despite the importance and interests in the topic of this article there seems to be a lack of experimental studies on the measurements of dynamic effects in heterogeneous porous sample. It is known that there are many types of heterogeneity, for example, fractures, microscale heterogeneities, layers, and so forth. Although there is clear indication that τ depends on the porous medium heterogeneity, most of these studies in this area are theoretical in nature involving numerical simulations[5,21] as far as the authors are aware of and there seems to be a lack of study which reports how to measure, and provides experimental evidence of, these dependencies. The present article aims to eliminate this gap by reporting an experimental study of the effects of heterogeneity on the dynamic effect in capillary pressure relationship for two-phase flow behavior. For the purpose of the article, a weakly layered porous domain is chosen as a model of heterogeneous porous sample where the contrast in permeability of various layers is not significant. These types of heterogeneity are easy to prepare in the laboratory and mimic real heterogeneity in the subsurface, for example, lamina, alternating layers of fine and coarse sand, and so forth.

Materials and Methods

Experimental approach

A previously reported experimental rig[7] has been used in this work to quantify the dynamic effects (τ) in the weakly heterogeneous (layered) porous media. The rig was originally used for determining dynamic effects in homogeneous porous media by Das and Mirzaei[7] who have discussed in detail the design and calibration of the rig and, the procedures for collecting experimental data. In the present case, the rig has been modified to include a cylindrical cell packed with a heterogeneous (layered) porous medium with three distinct layers (Figure 1) in which two-phase flow experiments are performed. The experiments involve injection of silicone oil at the top of the column through a hydrophobic filter and water drained out of the cell through a hydrophilic filter at the bottom of the cell. In consistent with our previous work,[4–7] the parameters that are determined for the purpose of calculating dynamic coefficient are the transient in situ water saturation (S), time derivative of the saturation ($\partial S/\partial t$), and the quasi-static ($P^{c,equ}$) and dynamic ($P^{c,dyn}$) capillary pressures. To obtain the water saturation (S), three mini time domain reflectometer (mini-TDR) probes are installed at different heights in the sample. Three pairs of pressure transducers (PTs) are also mounted on the cell wall, which are at the same heights as the mini-TDR probes. Each pair of PTs contains a PT equipped with hydrophilic filter and another with hydrophobic filter, which monitor average water (P_w) and oil (P_{nw}) pressures, respectively, corresponding to the saturation measurements by the TDR probes at the same heights. The differences in the pressure measurements ($P_{nw}^{dyn} - P_w^{dyn}$) are calculated to determine the local P^c at those heights. Locally measured water saturation and capillary pressure are then used to construct the dynamic and quasi-steady P^c–S curves, which are subsequently used to calculate the dynamic coefficient (τ) following Eq. 4.

Measurement sensors

In the experiments, three mini-TDR model T-3 probes (East 30 Sensors, Washington) are used for capturing water saturation (S) in the porous sample. TDRs are able to transform the electrical resistivity of the sample into values of water saturation (e.g., Das and Mirzaei[7]). The TDR probes are connected to an interface called multiplexer (Synchronous Device for Measurement, SDMX50, Campbell Scientific (CSI), Loughborough, UK). The multiplexer is connected to a TDR unit (TDR100, CSI, Loughborough, UK), which is then connected to the circuit board of the TDR100 unit to supply power, to enable the multiplexer and the

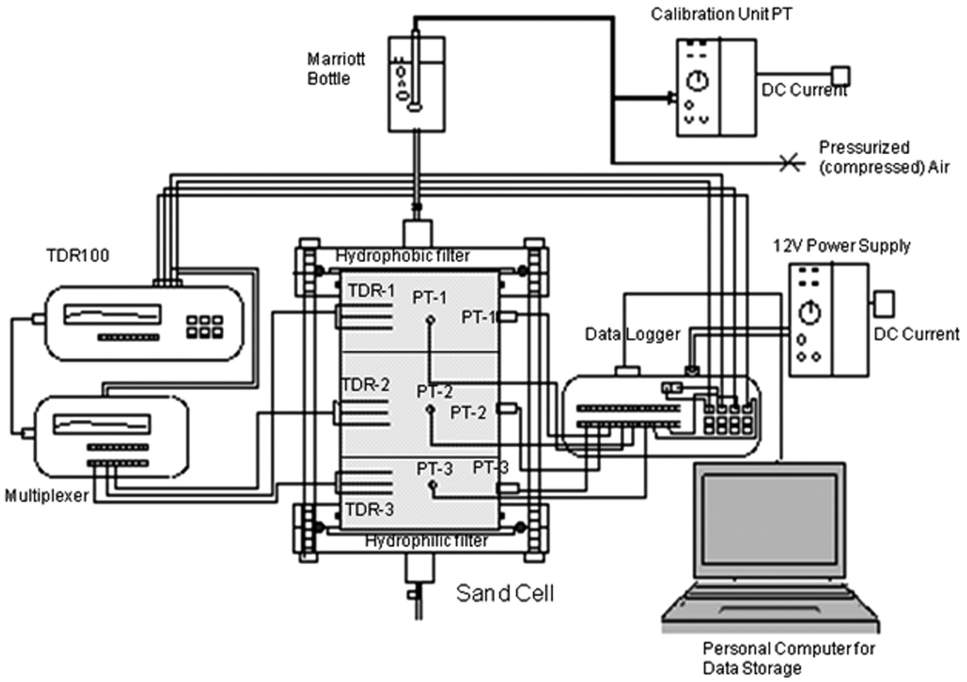

Figure 1. Experimental setup used to determine dynamic effects in heterogeneous porous domain.

(Adapted from Das and Mirzaei[7]).

probes to transfer the electrical pulse outputs to the TDR100 unit. The TDR100 unit is further cabled to a data logger (CR10X, CSI, Loughborough, UK) and computer with a software (PCTDR, CSI, Loughborough, UK) for automatic logging of the water saturation in the porous sample. The calibration of the TDR probes are discussed in detail by Das and Mirzaei[7] and is not discussed in this article. The same calibration procedures are followed for this work.

The pressures of the fluid phases are measured using six PTs (XTC-190M-7 BARG, Kulite Semiconductor Products, Leonia, NJ). To measure water pressures at different heights of the cell, three PTs are mounted on one side of the cell. Each PT is held in place by an acrylic holder to accommodate the filter flush with the inner wall of cell, in front of PT. There is a small space between a PT and the filter that allows water to accumulate in front of the PT for pressure measurement. To measure the pressure of the nonwetting phase (silicone oil), the PTs must to be modified as there is no standard PT that can measure these pressures directly. The modification was done by placing I-vyon F3.2 P4 treated (Porvair Technology, a division of Porvair Filtration Group, Wrexham, UK) polymeric filters in front of the PTs. Vyon is hydrophobic in nature and prevents aqueous solutions from wetting the pore structure of a filter. To make it hydrophilic, Porvair Technology applies special treatment process to enhance its surface wetting characteristics allowing immediate uptake of a wetting fluid and very high entry pressure for nonwetting fluid. The above modification allowed us to record the pressure of the nonwetting phase in the sample. All the PTs are connected to CR10X data logger for pressure data collection. The software LoggerNet 3.1 (CSI, Loughborough, UK) provides the facilities for communications, programming, data transfer, and data processing during the experiments as discussed by Das and Mirzaei.[7]

Properties of porous samples and fluids

The experiments in this work have been conducted using two commercial grades of silica sand, namely, Leighton Buzzard DA 14/25 as coarse-grained and Leighton Buzzard DA 30 as fine-grained sand (WBB Minerals, Cheshire, UK). Both sand types provide high uniformity of particle size (uniformity coefficient (d_{60}/d_{10}) = 1.32 for coarse and 1.21 for fine sand), sphericity and chemical purity. The average sizes of the coarse and fine sand particle are 946 and 482 μm, respectively. The sands are also low in organic matter content. In all the experiments, the fine and coarse sand samples are purged of air by stirring in a distilled water reservoir until no air bubble come out. The samples were also put in a vacuum unit to release any trapped air bubbles for 24 h. The experimental cell is then carefully mounted on a plate equipped with an o-ring to prevent any air inflow. A deaired and fully water saturated hydrophilic filter, used to facilitate water drainage and prevent oil flow at the outlet, is also placed at the bottom of the cell. Subsequently, the column is filled with distilled water. Wet and deaired sand is then poured into cell as described earlier. The whole unit is placed in a container to collect extra water. Visual observation is made to confirm that there is no air bubble in the sand pack following this procedure. The total mass of the sand inside the cell is recorded along with the volume of the cell and individual sand layers in the cell that allows calculation of porosity.

The two-phase flow experiments have been carried out in a cylindrical acrylic cell, 102 mm in diameter and 120 mm in length (Figure 1). To prepare the heterogeneous (layered) domain, a predefined mass of deaired and wet coarse sand is put in the cell to cover 3 mm above radius of influence of lowest mini-TDR probe. The radius of influence is the distance measured from outer probe rods, within which TDR reflection is not interfered with the reflection of other TDR

Table 1. Fluids and Porous Media Properties that are Relevant in this Study

Property	Coarse Sand	Fine Sand	Water	Silicone Oil
Permeability, K (m^2)	8.7×10^{-10}	3.1×10^{-10}	–	–
Porosity, θ	0.35	0.32	–	–
Entry pressure, P^d (N m^{-2})	510	675	–	–
Pore-size distribution index, λ	2.07	2.55	–	–
Residual water saturation, S_{rw}	0.258	0.271	–	–
Density, ρ (kg m^{-3})	–	–	1000	968
Viscosity, μ (kg m^{-1} s^{-1})	–	–	1×10^{-3}	193×10^{-3}
Surface tension, σ (N m^{-1})*	–	–	0.072†	0.035‡

The media properties are determined experimentally and the fluid properties are either standard values or taken from literature.
*As reported in Adamson and Gast.[29]
†Water–air system.
‡Silicone oil–water system.

probes and/or reflection of probe is not affected by the texture of sand out of radius of influence. It is defined by the manufacturer to be 3 mm for the type of the mini-TDR probes used. Subsequently, a known amount of fine sand is added to the cell to make a fine sand layer of 39-mm thickness to cover the middle mini-TDR probe. After this, another layer of coarse sand is deposited on the top of the find sand.

Only one configuration of heterogeneous domain may not be enough to draw a conclusion toward the effects of heterogeneity of porous media on the dynamic coefficient. Therefore, two heterogeneous domains are set up, which are named as heterogeneous domain #1 and heterogeneous domain #2. The difference between the two domains is the difference in the thickness of fine sand layer. In heterogeneous domain #2, fine sand layer is thicker. The maximum thickness of the fine sand layer depends on the spacing between mini-TDR probes. The cell is designed in a way so that the measurements from different mini-TDR probes do not interfere with one another. Therefore, the minimum thickness of fine sand layer must be more than the spacing between upper and lower rods of the mini-TDR probe, which is 22 mm. According to manufacturer's guidelines, a distance of 3 mm for upper and lower rods of each mini-TDR probe avoids interference with the signals of nearby rods of the other probes. Therefore, in heterogeneous domain #1, a layer thickness of 32 mm is chosen to cover mini-TDR probe and avoid the effect of the upper and lower coarse sand layers on the middle mini-TDR reading in the fine sand layer. The spacing between middle rods of two consecutive mini-TDR probes is defined to be 46 mm. Therefore, the maximum thickness of the fine sand layer is kept equal to 40 mm.

To keep the intensity of heterogeneity[2,4] in the domain the same, the identical amount of fine sand is added for each sample to make a layered domain. The top and bottom of fine sand layer is filled with a known amount of coarse sand, which covers the upper and the lower mini-TDR probes. To change the intensity of heterogeneity, the fine sand layer thickness is decreased to 30 mm, starting 10 mm above the upper rod of lower mini-TDR probe. Again, considering the distance between the subsequent probes and also radius of influence of each probe, a fine sand layer of 30-mm thickness will not affect the reflection of upper and lower mini-TDR probes, while it covers middle mini-TDR probe fully. The same mass of each type of sand is used in preparing samples with the same intensity of heterogeneity.

Before conducting a two-phase flow experiment, experiments involving single-phase flow using water under constant head were performed to measure intrinsic permeability of the sand pack. To perform this experiment, a hydrophilic filter was placed on the top of the sand column and inflow reservoir (Mariotte Bottle) was filled with distilled water. These are discussed in detail by Das and Mirzaei.[7] Properties of the fine and coarse sands, which include the intrinsic permeability, porosity, Brooks–Corey parameters[28] determined from quasi-static experimental results are listed in Table 1. The properties of fluids used in our experiments have also been presented in this table. The premises on which these tests take place are kept at a constant temperature of 20°C so as to avoid any influence of temperature variation on density, viscosity, and surface tension of the fluids used. Silicone oil (BDH Laboratory Supplies, Poole, UK) with viscosity of 200 cSt, which has negligible solubility in water, volatility at room-temperature, and health risk is selected as the nonwetting phase. The selected aqueous phase for our experiments is distilled water.

Procedures for quasi-static and dynamic two-phase flow experiments

To carry out the quasi-static and dynamic two-phase flow experiments, a Mariotte bottle filled with silicone oil is connected to the cell (Figure 1). This arrangement provides a constant pressure head for the flow of oil into the cell aided by a manual pressure regulator.

Quasi-Static Experiments. To conduct the quasi-static two-phase flow experiments, the outflow valve at the bottom of the cell is opened at first. The valve is leveled with the top of the sand to overcome hydrostatic head pressure gradient that minimizes the gravity effect. The initial pressure of silicone oil is zero within sand column. The pressure of silicone oil on the top column boundary is slowly increased by increasing the compressed air pressure on top of the Mariotte bottle. This leads to infiltration of silicone oil through a hydrophobic filter at the top of the cell. Injected oil displaces water out of the sand column (drainage). Water saturation (S) at different layers of the porous sample is directly measured using the three mini-TDR probes in the experimental cell. The flow experiments are carried out until a steady-state flow condition is reached, that is, the water flow rate stabilizes at the outflow valve ($\partial S/\partial t$). Measured S and P^c provide one point of a quasi-static P^c–S curve. Next, the imposed air pressure on the Marriot bottle, and hence the oil pressures, is increased, and the experiment is continued until a new steady state is reached, which provides another point for the P^c–S curve. This process is repeated several times to determine a complete P^c–S curve for a sample.

Dynamic Experiments. To conduct the dynamic two-phase flow experiments, the imposed silicone oil pressure at the top of domain is increased to a high pressure and kept constant by imposing a constant air pressure on Mariotte bottle. Table 2 shows the applied pressures for carrying out

Table 2. Boundary Conditions Used for Different Dynamic Two-Phase Flow in Cylindrical Homogeneous Porous Media Considering Pressure Cell Experiment Used for the Measurement of Dynamic Coefficient

		Top Boundary		Bottom Boundary	
Displacement Case	Time Duration (h)	Nonwetting Phase (Silicone Oil) Pressure (Pa)	Zero Flux Water	Water Pressure (Pa)	Zero Flux Nonwetting (Silicone Oil) Phase
Dynamic case 1	5.6	8		1.2	
Dynamic case 2	3.9	9		1.2	
Dynamic case 3	2.8	10		1.2	
Dynamic case 4	2.1	11		1.2	

different dynamic two-phase flow experiments in this work. The dynamic two-phase flow is continued until the saturation at lower TDR probe reaches its irreducible water saturation (S_i). The TDR probes measure the water content, whereas the PTs record oil and water pressure, as explained earlier. They provide the necessary data to determine three local dynamic P^c–S curves for each boundary pressure. Once the oil front reaches the bottom filter and lower mini-TDR probe start showing the irreducible saturation (S_i) the experiment is terminated. This experiment is repeated for four different conditions (8–11 kPa) to provide enough dynamic P^c–S curves that are then used with steady-state P^c–S curves to calculate the dynamic coefficient at the three different measurement heights within the column (discussed in the "Results" section).

Calculation of Dynamic Coefficient (τ). Equation 4 shows that if $P^{c,dyn} - P^{c,equ}$ and $\partial S/\partial t$ are known at a given saturation value, τ can be determined. Therefore, once the $P^{c,equ}$ and $P^{c,dyn}$ in different layers are determined, the data can be fitted to Eq. 4 to calculate the dynamic coefficient. This is a well-established procedure and has been used by a number of previous authors.[4,6,21] Also, as shown later, the τ–S curves in different layers follow a fairly consistent trend. We argue that one could average the τ–S data and calculate effective/average τ values as a function of average water saturation for the whole domain.[7] The average values are calculated using the following equations

$$\langle S\rangle = \frac{\sum_{i=1}^{i=n}(S|_{t_n})_{V_i}V_i}{\sum_{i=1}^{i=n}V_i} \tag{5}$$

$$\langle\tau\rangle|_{\langle S\rangle} = \frac{\sum_{i=1}^{i=n}(\tau\times S|_{t_n})_{V_i}V_i}{\sum_{i=1}^{i=n}(S|_{t_n})_{V_i}V_i}|_{\langle S\rangle} \tag{6}$$

where $\langle S\rangle$ is the volume-weighted water saturation that is also the average water saturation, $\langle\tau\rangle|_S$ is saturation weighted dynamic coefficient (τ), which is the average τ and presented as a function of average saturation. $(\tau)_{V_i}$ is the dynamic coefficient and $(S|_{t_n})_{V_i}$ is the measured saturation at a measurement volume V_i at the corresponding measurement height i, where $i = 1,2,3,\ldots,n$ is the number of measurements heights in which the τ–S curves are calculated, that is, the number of τ–S curves, in which $n = 3$.

Results and Discussion

Transient saturation (S–t) profiles

As discussed earlier in this article and by others,[6,7] the transient saturation (S–t) profiles are important in understanding the equilibrium/dynamic two-phase flow behavior in porous media. They show when the flow system reaches equilibrium ($\partial S/\partial t = 0$). Furthermore, S–t curves are needed to calculate $\partial S/\partial t$ and the dynamic coefficient according to Eq. 4. In addressing these issues, the transient saturation profiles for a typical oil pressure applied at the upper boundary of heterogeneous domain #1 are presented in Figures 2a,b. The first graph (Figure 2a) is for an oil pressure of 8 kPa at the upper boundary and uses the time elapsed from the start of the experiment. The figure shows that the residual water saturation at the middle layer, which is a fine sand layer with less permeability, is slightly higher than the upper and lower sand layers, which are made up of coarse sand with

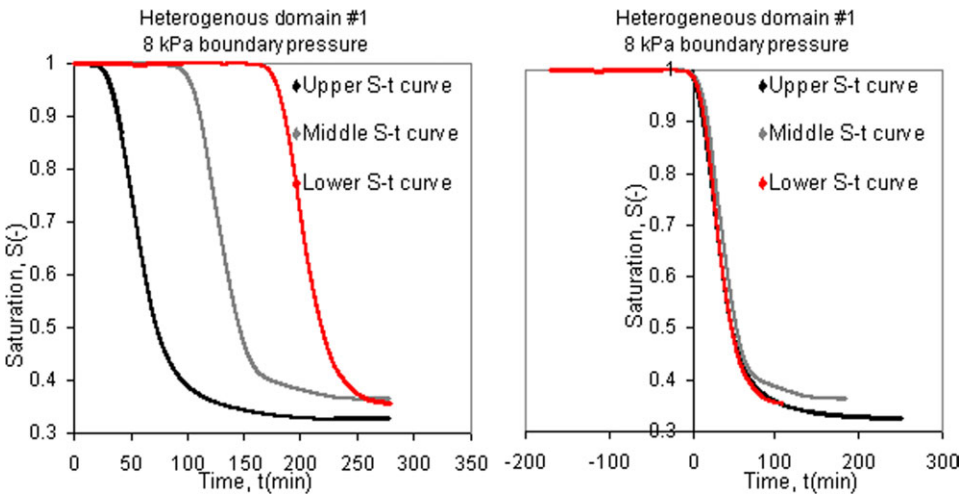

Figure 2. S–t curves in heterogeneous domain #1.

Panel (a) uses the time elapsed from the start of the experiment, whereas panel (b) uses the time from the moment the first change of saturation occurs. [Color figure can be viewed in the online issue, which is available at wileyonlinelibrary.com.]

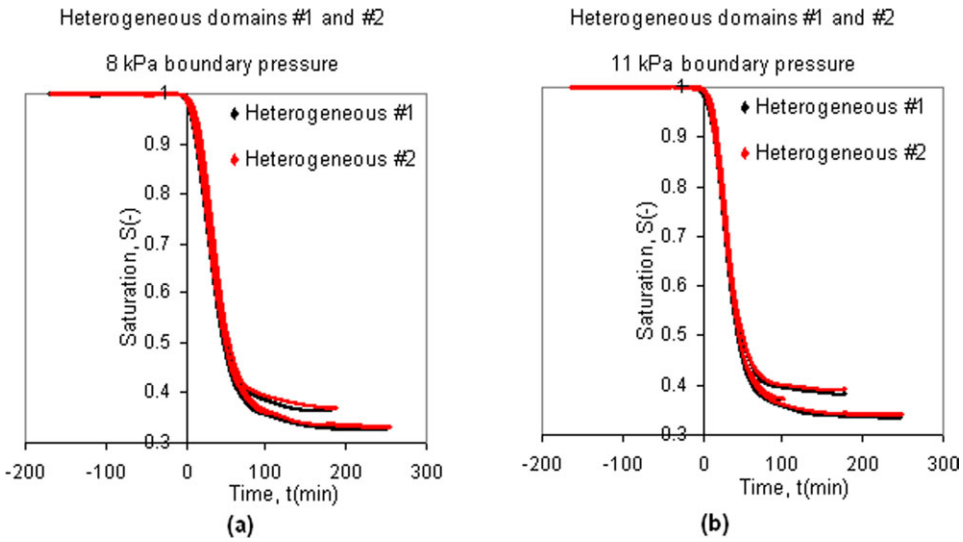

Figure 3. Comparisons of *S–t* curves in heterogeneous domains #1 and #2.

The figure uses the time from the moment the first change of saturation occurs. [Color figure can be viewed in the online issue, which is available at wileyonlinelibrary.com.]

higher permeability. This is due to the retention of higher amount of water in the fine sand layer as compared to the coarse sand layers. The *S–t* curves in this figure are superimposed and presented in Figure 2b for easy comparison of the *S–t* curves at different heights in the heterogeneous domain for 8 kPa boundary pressure. In effect, Figure 2b uses the time from the moment the first change of saturation occurs in different layers. As shown in this graph, the *S–t* curves in the upper and lower most layers almost overlie and follow similar trends, that is, rates of drainage in the two layers are similar at the same time. Further, there is a gap between these two curves and the *S–t* curve at the middle layer (fine sand). Obviously, this difference in saturation is related to the porous medium permeability. For the same boundary condition, it takes longer time for an oil to flow in fine sand than in coarse sand due to more resistance to the flow in fine sand. Similar trends in the *S–t* curves are observed for pressures of 9–11 kPa, which are not presented in this article due to lack of space. These results show that the saturation profiles at higher boundary pressure follow a similar trend with the residual saturation increasing with increasing the boundary pressure. Although some of these behaviors may be expected, it is important to quantify these values in this work so as to calculate the dynamic coefficient in different circumstances.

As in heterogeneous domain #1, the *S–t* curves for two-phase flow in heterogeneous domain #2 are presented in Figures 3a,b. As shown in this figure, the saturation profiles are similar at the beginning. However, as the experiment progresses and more water is displaced out of the cell by the injected silicone oil, the behavior of the saturation profiles change. These figures show that at all heights, the amount of the residual saturation in heterogeneous domain #2, with thicker fine sand layer, is higher than the residual saturation in heterogeneous domain #1. This implies that in heterogeneous domain #2, the residual water saturations are high not only in the fine sand layer but also the upper and lower coarse sand layers. This behavior again is due to trapping of more water in the fine sand layer. The amount of water being trapped as residual water increases as the volume of fine sand layer increases. Therefore, the saturation profiles in Figures 3a,b show that the amount of residual water in the thicker layer of fine sand in heterogeneous domain #2 is more than the amount of the residual water in heterogeneous domain #1. Similar behaviors are observed for boundary pressures of 9 and 10 kPa.

Quasi-static P^c–S *curves in different layers of a heterogeneous domain*

Having discussed the transient saturation profiles, the quasi-static P^c–S curves are presented in this section. The behaviors of quasi-static P^c–S relationships in homogeneous and heterogeneous porous domains are well understood and have been discussed earlier.[2,3,6,7] For example, Das et al.[3] have shown that there is a complex interplay of variables that affect the P^c–S curves in heterogeneous domain. Earlier, Das et al.[2] obtained similar results and showed that upscaled P^c–S curve mainly follows the corresponding curve for the background sand with the irreducible water saturation affected significantly by the medium properties and the amount of heterogeneity. The P^c–S curves obtained in this work are consistent in trends with those obtained in the previous studies (e.g., the curves have S-shapes) and are not discussed in length in this article. The P^c–S curves in different layers are presented for completeness of the discussion in this article, as they are needed for the calculation of dynamic coefficient. Figure 4 shows the P^c–S curves at the three measurement positions in heterogeneous domains #1 and #2. As shown in Figure 4, the P^c–S curves in the heterogeneous domain #2 are almost the same as the P^c–S curves in heterogeneous domain #1 for a large range of saturation. However, as the experiment progresses and water saturation decreases, the P^c–S curves in the heterogeneous domain #2 break away eventually and fall higher for lower saturation values implying that the water content in the heterogeneous domain #2 is higher at the same capillary pressure. This happens for almost all the boundary pressure values and the gap between the curves remains the same.

To demonstrate the reliability of the experimental data, the experimental data with oil pressure of 10 kPa at the top

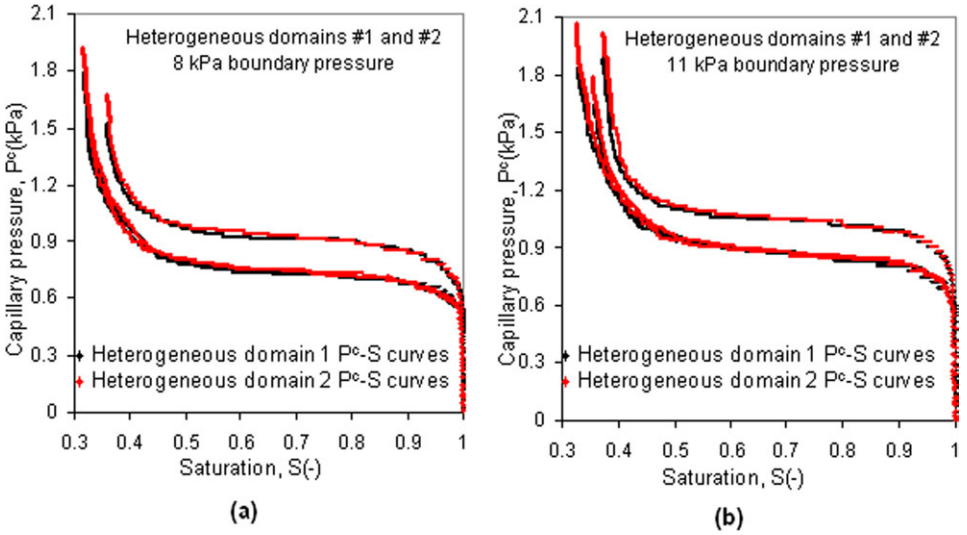

Figure 4. Comparisons of typical quasi-static P^c–S curves in heterogeneous domains #1 and #2.

[Color figure can be viewed in the online issue, which is available at wileyonlinelibrary.com.]

boundary of heterogeneous domains #1 is presented. The results of the original and repeated experiments are shown in Figure 5. As evident in this figure, the repeated results, shown with the red colored curves, overlap the original results. Figures 5a–c display the comparisons at the upper, middle, and lower layers of the sample, respectively. As

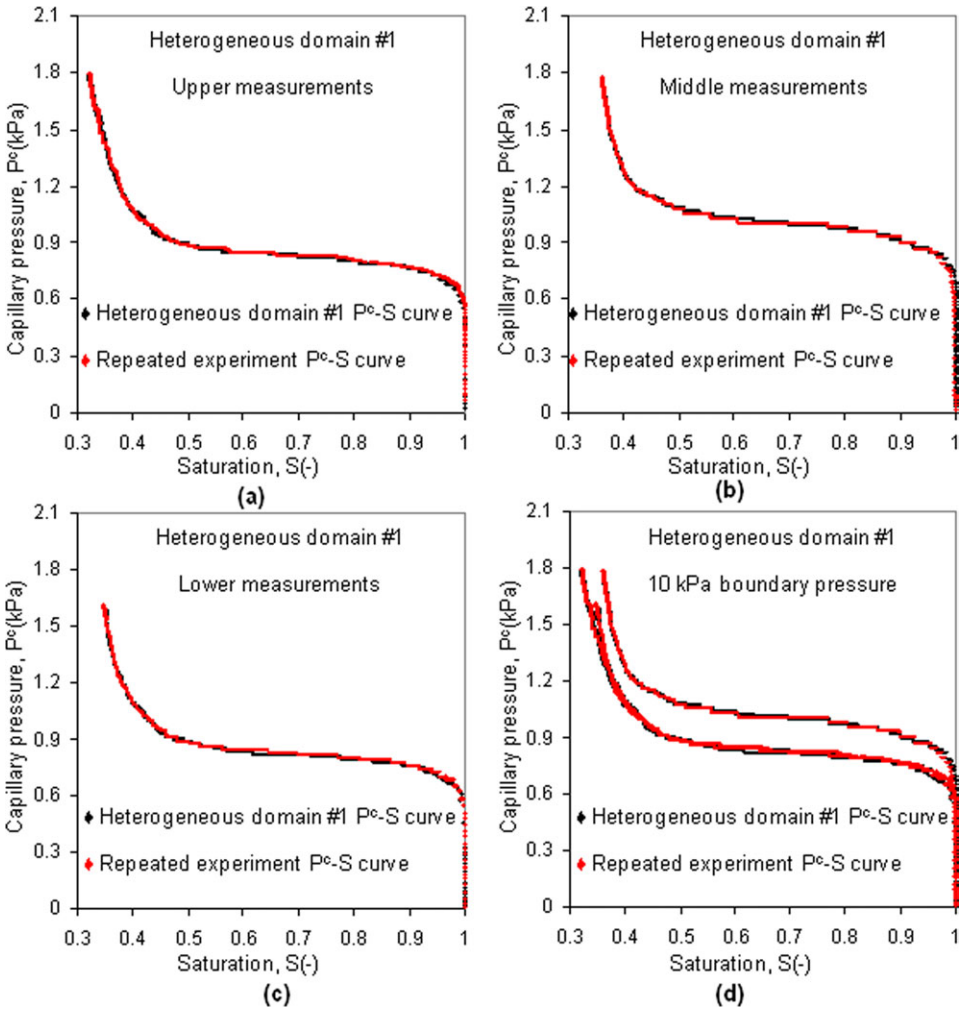

Figure 5. Results of repeated experiments in different layers of heterogeneous domain #1 for 10 kPa boundary pressure.

[Color figure can be viewed in the online issue, which is available at wileyonlinelibrary.com.]

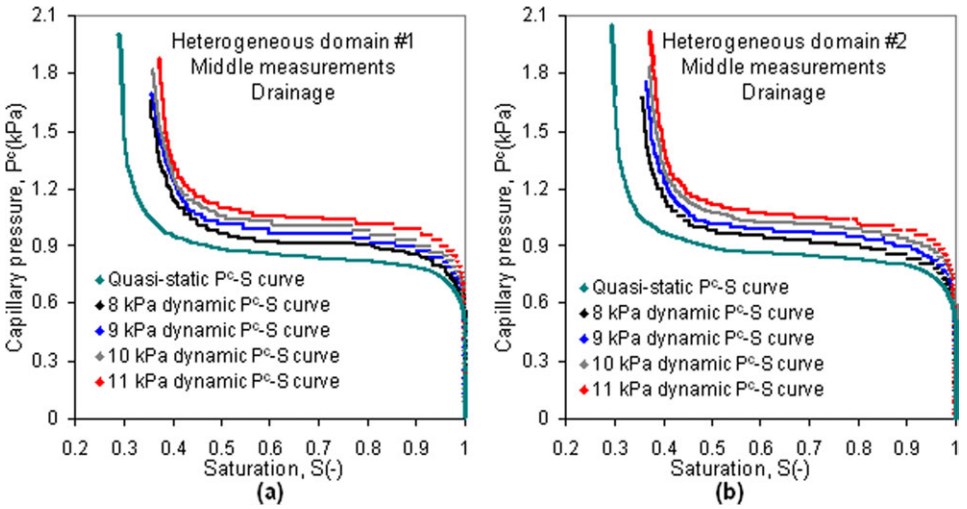

Figure 6. Drainage quasi-static and dynamic P^c–S curves at the middle measurement position (fine sand) of (a) heterogeneous domain #1 and (b) heterogeneous domain #2.

[Color figure can be viewed in the online issue, which is available at wileyonlinelibrary.com.]

displayed in these figures, the results are very similar, which give the confidence that the experiments have been conducted correctly and the results can be reproduced using the developed experimental rig. The data in Figures 5a–c are merged, and the resulting graphs are shown in Figure 5d to show that the overall trends in the two data sets are almost the same.

Dynamic and quasi-static P^c–S *curves in different layers*

Similar to the quasi-static P^c–S curves, the general trends of dynamic P^c–S curves have also been discussed earlier.[5,6,7,11] However, most of the studies in the area of this article (i.e., implications of heterogeneity on dynamic effects) are based on numerical simulations.[5,21] They show that the dynamic P^c–S curves fall above the quasi-static P^c–S curves for drainage. The experimental results obtained in this work are consistent with the predictions in the previous work. As an example of the results, Figure 6 is presented, which shows the dynamic and quasi-static P^c–S curves at the middle measurement position (fine sand) of the heterogeneous domains #1 and #2. As shown in the figure, the dynamic P^c–S curves lie above the quasi-static P^c–S curves. The same trends of data are obtained at the upper and lower heights of the sample (not shown in this article), which are then used to calculate the dynamic coefficient at different layers of the heterogeneous domain.

Time derivative of saturation in different layers

The next stage in the determination of the dynamic coefficient is to calculate the time derivatives of saturation ($\partial S/\partial t$) as a function of time (t), as they are needed for using Eq. 4. The significance of $\partial S/\partial t$–t curves has been described in detail by Das and Mirzaei.[7] Briefly, $\partial S/\partial t$ is the slope of the S–t curve and, as Das and Mirzaei[7] have shown, $\partial S/\partial t$ decreases and then increases with time until it is equal to zero when the two-phase flow system reaches equilibrium. As the saturation within the domain and $\partial S/\partial t$ change with time, the dynamic coefficient changes as well according to Eq. 4. This implies that the ease of reaching equivalence (dynamic coefficient) of the flow system should change with saturation and time along with any other factor (e.g., heterogeneity) that may affect $\partial S/\partial t$. Keeping in mind the importance of $\partial S/\partial t$–t relationships, the purpose of this section is to discuss briefly some of these results for heterogeneous domains.

Figure 7 compares the $\partial S/\partial t$–t curves of heterogeneous domains #1 and #2 for different boundary conditions. As shown earlier, there is not a big difference in the transient saturation profiles of heterogeneous domains #1 and #2 at the beginning of the experiments, when water saturation is high. Therefore, as shown in Figure 7a for oil pressure of 8 kPa applied at the top boundary, the $\partial S/\partial t$–t curves for heterogeneous domain #2 are very close to the $\partial S/\partial t$–t curves for heterogeneous domains #1. For a closer comparison, the graphs at different measurement heights at each heterogeneous case are superimposed and displayed in Figure 7b. As shown in this figure, the $\partial S/\partial t$–t curves almost overlap. However, a magnified version of this figure shows that the minimum value of $\partial S/\partial t$ in heterogeneous domain #2 is slightly lower than that of heterogeneous domain #1. This may be attributed to the higher amount of fine sand in heterogeneous domain #2 leading to smaller values of $\partial S/\partial t$. Figures 7c,d show the $\partial S/\partial t$–t curves in heterogeneous domains #1 and #2 for 10 and 11 kPa boundary pressures. The graphs have similar behavior to the graphs for 8 kPa boundary pressure.

Dynamic coefficients in different layers of the same domain

Having examined the P^c–S curves and saturation profiles in heterogeneous domains #1 and #2, the aim of this section is to discuss the measured dynamic coefficient (τ) in the heterogeneous domains. As is the convention in the published literature (e.g., Refs. 7 and 18), the dynamic coefficients are presented as τ–S curves. To begin with, the coefficients in different layers of heterogeneous domain #1 are determined and compared with the τ–S data of the corresponding heights in homogeneous domain of Das and Mirzaei[7] keeping all other factors (e.g., boundary pressure, fluid properties, and porous medium type) the same. Das and Mirzaei[7] have

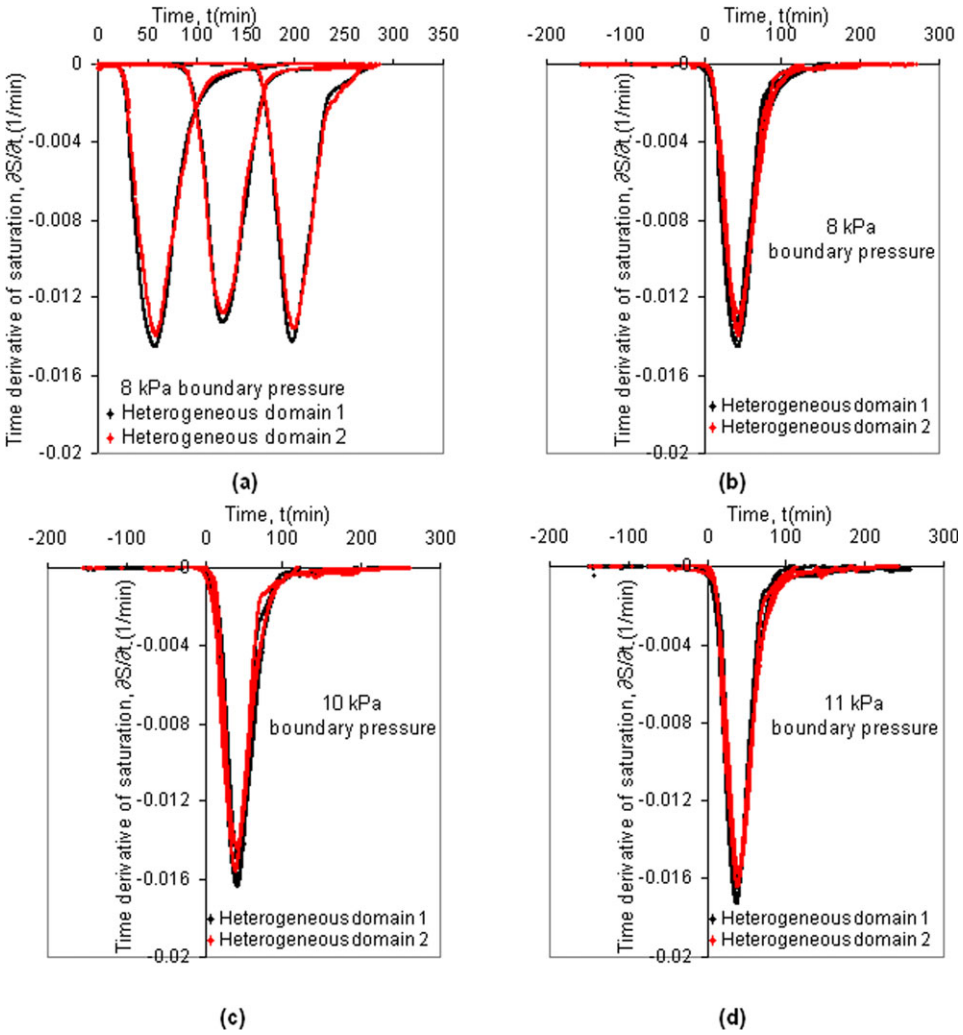

Figure 7. Comparisons of typical $\partial S/\partial t$–t curves in heterogeneous domains #1 and #2.

Panel (a) uses the time elapsed from the start of the experiment, whereas panels (b)-(d) use the time from the moment the first change of saturation occurs. [Color figure can be viewed in the online issue, which is available at wileyonlinelibrary.com.]

presented τ–S curves for homogeneous coarse and fine sand, which have the same material properties (e.g., porosity and permeability) as used in this work. Therefore, the τ–S data of the coarse sand layer (upper and lower layers) in heterogeneous domain #1 are compared with the τ–S data at the corresponding heights (i.e., upper and lower layers) of coarse sand in the experimental cell.[7] Similarly, the τ–S data of the fine sand layer (middle layer) in heterogeneous domain #1 are compared with the τ–S data at the middle of homogeneous fine sand, which are presented by Das and Mirzaei.[7] This approach of comparing the τ–S curves for the same porous medium and fluid properties as well as the heights is adopted, as these factors are known to affect the τ values. For example, it was suggested by Das and his coworkers[4,5,7] that the dynamic effect, and hence the rate at which a two-phase flow system reaches equilibrium, at a location may depend on its distance from the boundary of the domain where fluid is injected. By adopting the above approach of comparing the τ–S data in heterogeneous and homogenous domains, we expect that the difference in the τ–S data can be attributed to the layers in the heterogeneous domain alone and not anything else. Consequently, it is envisaged that the comparison method adopted in this work would provide a better understanding of the dynamic effects in the heterogeneous domain.

The graphs in Figures 8a–c show such a comparison. Figure 8a shows the τ–S data at the upper most measurement position of a homogeneous coarse sand domain[7] and heterogeneous domain #1. As is clear from this figure, the τ–S data at the upper measurement position of the heterogeneous domain overlie the τ–S data at the upper measurement height of the coarse sand domain. However, at lower saturation values, the two data sets do not match, and the τ–S data in the heterogeneous domain break away and lie above. We have already observed in our experiments that for higher saturation values, both the $\partial S/\partial t$–t and local P^c–S curves in heterogeneous domain are identical to the curves at the corresponding positions in homogeneous domain. Therefore, it is not surprising that the τ–S data calculated from the local curves in homogeneous and heterogeneous domains overlie initially. However, the τ–S curve for the coarse sand in the heterogeneous domain break away from the corresponding curves in homogeneous coarse sand domains at lower saturation values due to the heterogeneity effects on the time to flow equilibrium. Figure 8b shows a comparison of the τ–S data at the middle measurement height of heterogeneous

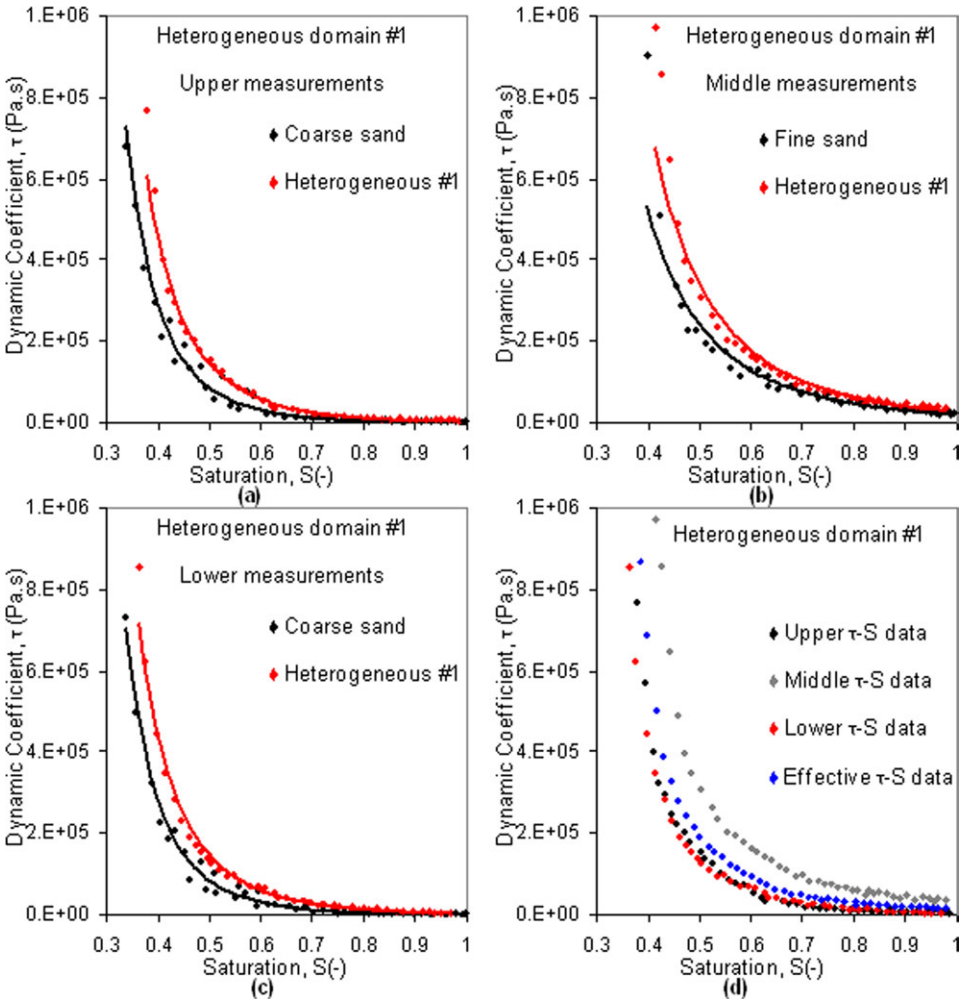

Figure 8. (a) τ–*S* curves at upper measurement height of homogeneous coarse sand and heterogeneous domain #1, (b) τ–*S* curves at middle measurement height of homogeneous fine sand and heterogeneous domain #1, (c) τ–*S* curves at lower measurement height of homogeneous coarse sand and heterogeneous domain #1, and (d) the τ–*S* curves at three measurement heights of heterogeneous domain #1 and the effective τ–*S* curve.

[Color figure can be viewed in the online issue, which is available at wileyonlinelibrary.com.]

domain #1 and homogeneous fine sand domain.[7] As in Figure 8a, the two curves overlie at the beginning but as saturation decreases, the τ–*S* data in heterogeneous domain break away and lie higher implying that the time to equilibrium in the fine sand in a heterogeneous domain is likely to be higher than a homogenous fine sand sample at the same saturation. Figure 8c displays the τ–*S* data at the lower measurement height of homogeneous coarse sand[7] and heterogeneous domain #1. The data follow a similar trend to the τ–*S* data in Figure 8a. Figures 8a–c show that the τ–*S* data in heterogeneous domain #1 follow a "power law" functional dependence.

Effective dynamic coefficient–saturation (τ–S) relationships for layered domain

Having calculated the τ–*S* data at the three measurement heights in the heterogeneous domains, the effective τ–*S* data for heterogeneous domain are calculated using Eqs. 5 and 6. The dynamic coefficient is known to vary depending on the scale of the domain, increasing with the increase in the domain size. The coefficient also depends on material properties, saturation, and so forth. As evident in the Eqs. 5 and 6, the porosity and volumes of the sand layers around each measurement position are considered to calculate the average τ–*S* data. Figure 8d shows the τ–*S* data calculated at the three measurement heights in different layers and the average values of these data points. As shown in this figure and discussed in earlier paragraphs, the τ–*S* data at the upper and lower measurement heights almost overlie while the τ–*S* data at the middle measurement height lie slightly higher. This means that in the layers of heterogeneous domains (core scale), the equivalence of the two-phase flow system would be established more or less at the same time provided all other factors (e.g., material and fluid properties and size of layer) are the same. However, the displacement in a different layer (e.g., a middle layer made of fine sand) is likely to need different equilibrium time to reach quasi-static condition due to variation in material properties.

Figure 8d also shows that the effective τ–*S* values are closer to the τ–*S* data calculated at the upper and lower layers made up with coarse sand. This is logical, because the maximum volume of the heterogeneous domain is occupied by the

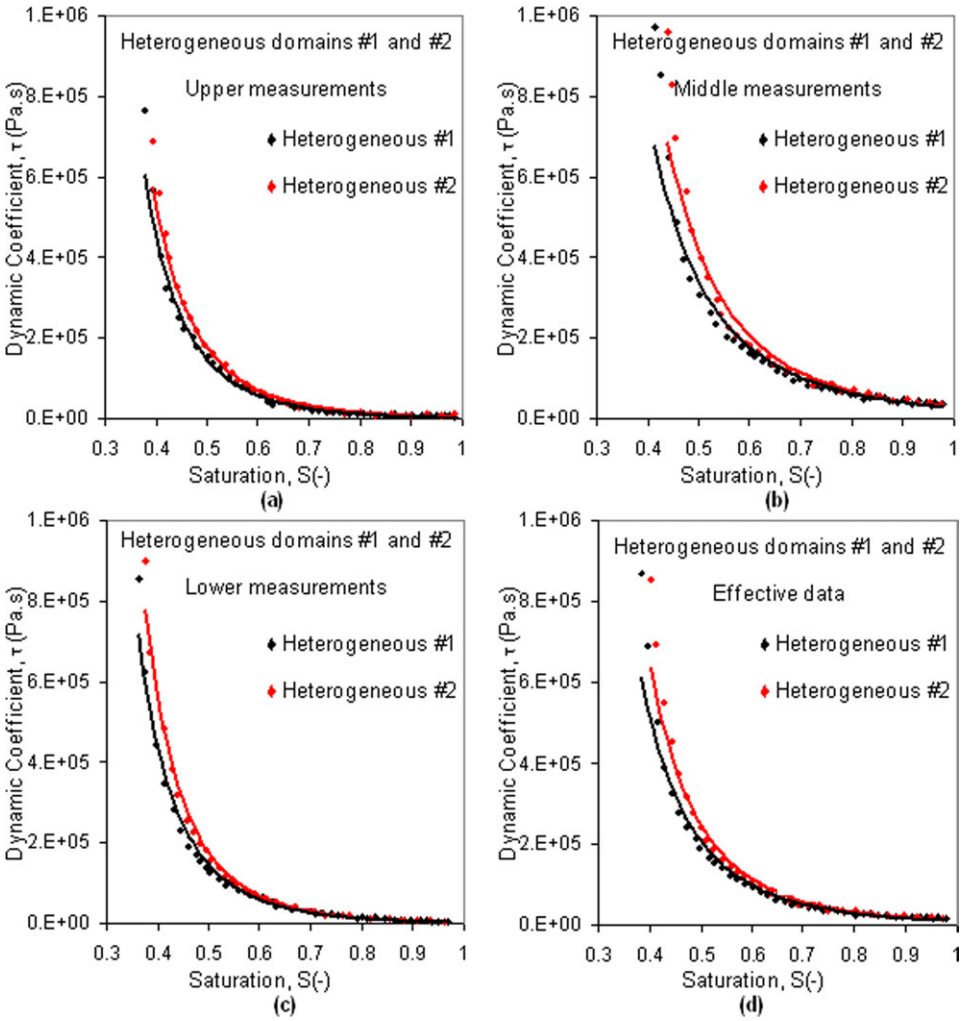

Figure 9. (a) τ–S curves at upper measurement height, (b) τ–S curves at middle measurement height, (c) τ–S curves at lower measurement height of heterogeneous domains #1 and #2, and (d) the effective τ–S curves for heterogeneous domains #1 and #2.

[Color figure can be viewed in the online issue, which is available at wileyonlinelibrary.com.]

coarse sand. In general, this figure suggests that the effective dynamic coefficient for a heterogeneous domain is affected by the porous media type that has occupied higher portion of the total volume, for example, the coarse sand in this case. In terms of the dynamic coefficient, Figure 8d shows that although the τ values at the upper or lower layers in the heterogeneous domain are almost the same, the average τ value may be higher than these values due to the presence of fine sand. However, the τ values are less than those for the homogeneous fine sand layer (middle layer) at the same saturation.

Dynamic coefficient–saturation (τ–S) relationships for different layered domains

Having compared the τ–S data at different measurement heights in heterogeneous domain #1 with the τ–S data at the corresponding heights in homogeneous domains, the τ–S data for heterogeneous domains #1 and #2 are compared to assess further the effects of heterogeneity (i.e., the variation in the thickness of fine sand layer) on the local and effective τ–S relationships. Figures 9a–c show the τ–S data at the upper, middle, and lower measurement heights of heterogeneous domains #1 and #2, respectively. These figures show that at higher saturation values, the τ–S relationships in heterogeneous domain #2 are almost identical to the corresponding data in heterogeneous domain #1. However, the τ–S data in heterogeneous domain #2 may lie above the corresponding data in heterogeneous domain #1 for lower range of the saturation values. This implies that as the water saturation decreases in the domains with higher amount of find sand, the flow system needs more relaxation time to reach equilibrium. A comparison between the individual pair of curves of each domain at the same measurement position shows that the general trend of the τ–S data at the upper and lower measurement heights are not significantly different. The difference in the τ–S data in the middle measurement height is slightly more pronounced. Considering, the increased thickness of the fine sand layer in heterogeneous domain #2, this behavior is expected. Also, the τ–S data in all the measurement heights in heterogeneous domain #2 lie higher than the τ–S data for heterogeneous domain #1. This seems to suggest that the effects of the fluid and material (e.g., heterogeneity and permeability) properties on the dynamic coefficient at a position in a laboratory scale domain dominate any affect of that the distance of the measurement position from the fluid injection point.

To make a better comparison between the τ–S data in heterogeneous domains #1 and #2 and assess the effect of the heterogeneity on the dynamic coefficient, the effective τ–S data of the two domains are presented in Figure 9d. This figure shows that although the differences in the effective τ–S data for the two cases are negligible for higher saturation, the data sets follow slightly different trends at lower saturations in consistent with the observation for local τ–S data at different heights. This means that the two domains need different relaxation times to reach the quasi-static conditions as water saturation decreases during a drainage process. The dynamic coefficient in the domain with the higher intensity of heterogeneity (i.e., higher amount of fine sand) is higher, which is in line with the numerical results obtained previously.[5] The comparison clearly shows that the presence of heterogeneities in the domain affects the dynamics of the two-phase flow behavior.

Conclusions

In this work, well-defined laboratory experiments have been carried out to determine the significance of dynamic effects in capillary pressure relationships for two-phase flow in weakly layered porous media. In consistent with the previous studies, the dynamic effect is indicated by a dynamic coefficient (τ), which establishes the speed at which flow equilibrium ($\partial S/\partial t = 0$) is reached. The data presented are for domains that contain a fine sand layer sandwiched between two coarse sand layers. It is clear that τ is a nonlinear function of saturation in heterogeneous domains, which is consistent with most numerical studies done before on the subject. τ is also found to increase in the regions of less permeability (fine sand). However, the effective τ–S data for the whole domain are dominated by the τ–S curves for coarse sand, as it occupies the maximum volume in the sample used for our experiments.

Acknowledgments

This study has been carried in the framework of the EPSRC (UK) Project GR/S94315/01, microheterogeneity and temperature effects on dynamic capillary pressure–saturation relationships for two-phase flow in porous media. The EPSRC funding for this project is gratefully acknowledged. Prof. G. Sills (the University of Oxford, Oxford, UK) is acknowledged for her contribution in completing the experiments in this work.

Literature Cited

1. Tsakiroglou CD, Theodoropoulou MA, Karoutsos V. Nonequilibrium capillary pressure and relative permeability curves of porous media. *AIChE J*. 2003;49(10):2472–2486. DOI: 10.1002/aic.690491004.
2. Das DB, Hassanizadeh SM, Rotter BE, Ataie-Ashtiani B. A numerical study of micro-heterogeneity effects on upscaled properties of two-phase flow in porous media. *Transp Porous Media*. 2004;56:329–350.
3. Das DB, Mirzaei M, Widdows N. Non-uniqueness in capillary pressure–saturation–relative permeability relationships for two-phase flow in porous media: implications of intensity and random distribution of micro-heterogeneity. *Chem Eng Sci*. 2006;61:6786–6803.
4. Das DB, Gauldie R, Mirzaei M. Dynamic effects for two-phase flow in porous media: fluid property effects. *AIChE J*. 2007;53(10):2505–2520. DOI: 10.1002/aic.11292.
5. Mirzaei M, Das DB. Dynamic effects in capillary pressure–saturations relationships for two-phase flow in 3D porous media: implications of micro-heterogeneities. *Chem Eng Sci*. 2007;62:1927–1947.
6. Hanspal N, Das, DB. Dynamic effects on capillary pressure–saturation relationships for two-phase porous flow: implications of temperature. *AIChE J*. 2012;58(6):1951–1965. DOI: 10.1002/aic.12702.
7. Das DB, Mirzaei M. Dynamic effects in capillary pressure relationships for two-phase flow in porous media: experiments and numerical analyses. *AIChE J*. 2012;58(6):1951–1965. DOI: 10.1002/aic.12702.
8. Hanspal N, Allison B, Deka L, Das DB. Artificial neural network (ANN) modeling of dynamic effects on two-phase flow in homogeneous porous media. *J Hydroinform*. In press.
9. Darcy H. *Les Fontaines Publiques de la Ville de Dijon*. Paris: Victor Dalmont, 1856.
10. Bear J, Verruijt A. *Modeling Groundwater Flow and Pollution*. Dordrecht, The Netherlands: D. Reidel Publishing Company, 1987.
11. Hassanizadeh SM, Celia MA, Dahle HK. Dynamic effect in the capillary pressure–saturation and its impact on unsaturated flow. *Vadose Zone J*. 2002;1:38–57.
12. O'Carroll DM, Mumford KG, Abriola LM, Gerhard JI. Influence of wettability variations on dynamic effects in capillary pressure. *Water Resour Res*. 2010;46:W08505.
13. Hassanizadeh SM, Gray WG. Thermodynamic basis of capillary pressure in porous media. *Water Resour Res*. 1993;29(10):3389–3405.
14. Mumford KG, O'Carroll DM. Drainage under nonequilibrium conditions: exploring wettability and dynamic contact angle effects using bundle-of-tubes simulations. *Vadose Zone J*. 2011;10(4):1162–1172. DOI: 10.2136/vzj2010.0125.
15. O'Carroll DM, Phelan TJ, Abriola LM. Exploring dynamic effects in capillary pressure in multistep outflow experiments. *Water Resour Res*. 2005;41:W11419.
16. Camps-Roach G, O'Carroll DM, Newson TA, Sakaki T, Illangasekare TH. Experimental investigation of dynamic effects in capillary pressure: grain size dependency and upscaling. *Water Resour Res*. 2010;46:W08544.
17. Juanes R. Nonequilibrium effects in models of three-phase flow in porous media. *Adv Water Res*. 2009;31:661–673.
18. Joekar-Nisar V, Hassanizadeh SM. Effect of fluids properties on non-equilibrium capillarity effects: dynamic pore-network modeling. *Int J Multiphase Flow*. 2011;37:198–214.
19. Joekar-Nisar V, Hassanizadeh SM, Dahle HK. Non-equilibrium effects in capillarity and interfacial area in two-phase flow: dynamic pore-network modeling. *J Fluid Mech*. 2010;655:38–71.
20. Goel G, O'Carroll DM. Experimental investigation of nonequilibrium capillarity effects: fluid viscosity effects. *Water Resour Res*. 2011;47:W09507. DOI: 10.1029/2010WR009861.
21. Manthey S, Hassanizadeh SM, Helmig R. Macro-scale dynamic effects in homogeneous and heterogeneous porous media. *Transp Porous Media*. 2005;58(1–2):121–145.
22. Civan F. Temperature dependency of dynamic coefficient for nonequilibrium capillary pressure–saturation relationship. *AIChE J*. 2012;58(7):2282–2285. DOI: 10.1002/aic.13817.
23. Bottero S, Hassanizadeh SM, Kleingeld PJ, Heimovaara TJ. Nonequilibrium capillarity effects in two-phase flow through porous media at different scales. *Water Resour Res*. 2011;47:W10505. DOI: 10.1029/2011WR010887.
24. Gray WG, Miller Cass T. TCAT analysis of capillary pressure in non-equilibrium, two-fluid-phase, porous medium systems. *Adv Water Resour*. 2011;34(6):770–778. DOI: 10.1016/j.advwatres.2011.04.001.
25. Peszynska M, Yi SY. Numerical methods for unsaturated flow with dynamic capillary pressure in heterogeneous porous media. *Int J Numer Anal Model*. 2008;5:126–149 (Special Issue).
26. Fucik R, Mikyska J, Sakaki T, Benes M, Illangasekare TH. Significance of dynamic effect in capillarity during drainage experiments in layered porous media. *Vadose Zone J*. 2010;638 9(3):697–708.
27. Sakaki T, O'Carroll DM, Illangasekare TH. Direct quantification of dynamic effects in capillary pressure for drainage-wetting cycles. *Vadose Zone J*. 2010;9(2):424–437.
28. Brookes RH, Corey AT. *Hydraulic Properties of Porous Media. Hydrology Paper*, Vol. 3. Fort Collins: Civil Engineering Department, Colorado State University, 1964.
29. Adamson AW, Gast AP. *Physical Chemistry of Surfaces*, 6th ed. New York: Wiley-Interscience Publications, 1997:784. ISBN 0-471-14873-3.

Manuscript received Feb. 7, 2012, and revision received July 30, 2012.